JOURNAL OF SPACECRAFT AND ROCKETS
Vol. 37, No. 6, November–December 2000

Hypervelocity Skin-Friction Reduction by Boundary-Layer Combustion of Hydrogen

C. P. Goyne,* R. J. Stalker,† and A. Paull‡
University of Queensland, Brisbane, Queensland 4072, Australia
and
C. P. Brescianini§
Commonwealth Scientific and Industrial Research Organization, North Ryde, Sydney, New South Wales 2113, Australia

Shock-tunnel measurements of Stanton number and skin-friction coefficient are reported for the injection of hydrogen through a 1.6-mm slot into a turbulent boundary layer in a 1-m-long duct. The mainstream Mach number of 4.5, stagnation enthalpy of 7.8 MJ/kg, pressure of 50 kPa, and temperature of 1500 K provided a combination of flow variables that was sufficient to ensure boundary-layer combustion of the hydrogen. The experiments were also simulated by a numerical model. The experiments and the numerical model indicated that the Stanton number was only slightly affected by boundary-layer combustion. However, the numerical simulation indicated that injection with combustion caused a reduction of approximately 50% in the skin-friction coefficient, whereas the experiments yielded an even greater effect, with the reduction in skin-friction coefficient reaching 70–80% of the values of skin friction with no injection. Numerical simulation of a constant pressure flow indicated that boundary-layer combustion caused the skin-friction reduction to persist for at least 5 m downstream.

Nomenclature

c_f	=	local skin-friction coefficient
c_h	=	local Stanton number
H_s	=	stagnation enthalpy, MJ/kg
H_w	=	wall enthalpy, MJ/kg
l	=	spanwise length of injection slot, m
$\dot{m}_i$	=	injected H_2 mass flow, kg/s
p	=	local static pressure, kPa
$\dot{q}$	=	surface heat transfer rate, MW/m^2
U	=	mainstream velocity, m/s
V	=	skin-friction gauge output
V_{HT}	=	skin-friction gauge output due to heat transfer
V_p	=	skin-friction gauge output due to pressure
V_s	=	skin-friction gauge output due to skin friction
γ	=	ratio of specific heats
ρ	=	mainstream density, kg/m^3
τ	=	local surface shear, Pa

Subscripts

n	=	no injection condition
0, 180	=	skin-friction gauge orientation

Introduction

HYPERVELOCITY flight in both cruise and boost modes will require vehicles with a slender configuration, and boundary-layer effects can be expected to offer formidable obstacles to the realization of such vehicles. Boundary-layer effects can also be expected to reduce the performance of vehicles in the glide mode considerably. These effects include not only high surface heat transfer rates, but also high levels of skin-friction drag.

The importance of skin-friction drag can be illustrated by considering a flat plate at incidence at high Mach numbers. For example, at a flight Mach number of 16 with a turbulent boundary layer and a mean skin-friction coefficient on the windward surface of 1.7×10^{-3}, it is found that the skin-friction drag is equal to the inviscid drag at an angle of incidence of 7 deg. Thus, for a vehicle with a configuration approximating a simple 7-deg wedge, with the windward surface at an incidence of 7 deg, it can readily be shown that skin-friction drag can halve the ratio of lift to drag, with attendant reductions in the range or the landing footprint of the vehicle. At lower angles, skin-friction effects will be even greater. Therefore, it comes as no surprise to find that skin-friction drag also seriously compromises the performance of a scramjet vehicle. This has been demonstrated by shock-tunnel experiments on a simple model designed for cruise propulsion at 2.45 km/s with hydrogen fueled scramjets,[1] where it was found that 49% of the fuel-off drag was due to skin friction. Clearly reduction of skin-friction drag is an important requirement of hypervelocity flight.

One method of accomplishing this reduction is to inject gas along the wall. The reduction in heat transfer when gas is injected through a slot has been the subject of a number of investigations.[2–5] The effect of a number of different injected gases with a laminar boundary layer at hypersonic Mach numbers was studied[5] and, from a theoretical correlation of the results, it was concluded that hydrogen was the most effective coolant. This agreed with the results of other experiments,[3] where a number of gases, including hydrogen, were injected into a hypersonic turbulent boundary layer. In both of these cases, the flow conditions were such as to preclude combustion of the hydrogen.

Skin-friction reduction with gas injection has also received attention. Experiments involving a supersonic mainstream have been performed on a porous plate with nitrogen injection,[6] on the injection of air and helium through a slot and through a porous wall,[7,8] and on the injection of air and helium through a slot.[8] These experiments demonstrated that helium was more effective than air in reducing skin friction. A numerical calculation[9] with air injection, and experiments at Mach 6 (Ref. 10), showed that the downstream length over which skin friction was reduced, as well as the magnitude of the proportional reduction, was at least as great as the proportional reduction in heat transfer. Because hydrogen has a lower viscosity and density than helium, it might be hoped that it would yield greater proportional reductions in skin friction than helium and that it would also follow the results in Ref. 3 for heat transfer, in yielding a greater downstream extent of skin-friction reduction than any other gas.

The use of hydrogen is efficient because it is the preferred fuel for hypervelocity propulsion. However, boundary-layer temperatures generated in hypervelocity flight can lead to combustion in the

Received 21 October 1999; revision received 8 June 2000; accepted for publication 13 June 2000.

*Postgraduate Scholar, Department of Mechanical Engineering; currently Research Associate, Department of Mechanical and Aerospace Engineering, University of Virginia, Charlottsville, VA 22901.
†Emeritus Professor, Department of Mechanical Engineering. Associate Fellow AIAA.
‡Senior Research Fellow, Department of Mechanical Engineering.
§Research Scientist, Division of Building, Construction and Engineering.

boundary layer, and it is uncertain how this will affect both the heat transfer and the skin friction.

This paper reports a shock-tunnel investigation of slot injection of hydrogen in a turbulent hypervelocity boundary layer, under conditions such that combustion occurs, together with a numerical simulation of the experimental situation. Such a study, involving pressure and heat transfer measurements, has been reported previously.[11] The present investigation is aimed at extending the previous study to include the skin friction. The following sections describe the experimental arrangement and measurements of the distributions of pressure, heat transfer, and skin friction along a constant area duct. The numerical simulation of the flow is then briefly described, and the experimental results for heat transfer and skin friction with boundary-layer combustion are compared with the results of the simulation. Discussion of the comparison then precedes the conclusion.

Experiment

Shock Tunnel and Test Conditions

The experiments were performed in the free piston reflected shock tunnel T4 at the University of Queensland. This tunnel incorporates a free piston driver, 229 mm in diameter and 26 m long, with a shock tube 75 mm in diameter and 10 m long.[12] A contoured axisymmetric nozzle, with a 25-mm-diam throat and 135-mm exit diameter, was located at the downstream end of the shock tube and produced a freejet with a pitot profile uniform within ±4% over a core diameter of 100^{+10}_{-0} mm. After expansion through the nozzle, the test flow passed to the entry of the experimental duct, as shown in Fig. 1.

The test conditions were calculated by using the shock speed and the shock tube filling pressure to yield the conditions after shock reflection and then by assuming an isentropic expansion to the pressure measured at a station 62 mm upstream of the end of the shock tube. This result yielded the nozzle stagnation enthalpy; then a one-dimensional nonequilibrium nozzle expansion to the measured test section pitot pressure provided the test conditions summarized in Table 1. It was noted that the test duration was reduced with an increase in stagnation enthalpy,[13] and so conditions were chosen to yield the maximum stagnation enthalpy consistent with a duration of 2 ± 0.4 ms after arrival of flow in the test section. The test flow composition in Table 1 is that given by the calculations, although experiments[14] indicate that there is doubt concerning the values given, particularly in the case of atomic oxygen.

Table 1 Shock-tunnel flow conditions[a]

Quantity	Units	Error, %	Test flow	Duct entry section	Test duct (no injection)
Stagnation enthalpy	MJ kg^{-1}	+4, −8	7.8	——	——
Nozzle supply pressure	MPa	±5	30.9	——	——
Mach no.	——	——	4.31	4.25	4.52
Temperature	K	+4, −8	1640	1660	1500
Pressure	kPa	±8	75	75	51
Density	kg m^{-3}	±13	0.159	0.155	0.116
Velocity	m · s^{-1}	+2, −4	3340	3330	3380
Pitot pressure	MPa	±6	1.67	——	——
Unit Reynolds no.	m^{-1}	——	——	8.8×10^6	——

[a]Composition: 0 mol fraction 1.2%, NO mol fraction 6.4%.

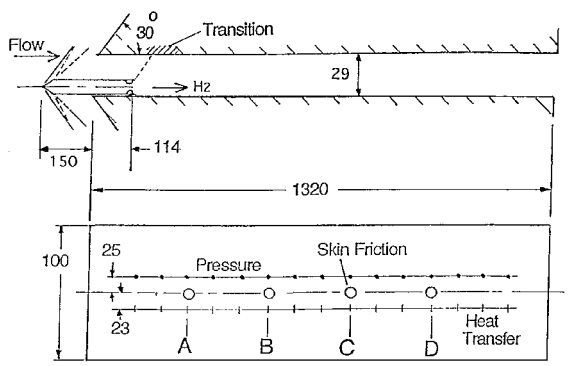

Fig. 1 Experimental duct (dimensions in millimeters).

Figure 2 presents typical test records showing that steady flow is obtained during the test time. The Reynolds number of the mainstream flow at the station of the hydrogen injection was 2.3×10^6; therefore, the boundary layer in the test duct was turbulent.

Experimental Duct

The experimental duct is shown schematically in Fig. 1. Hydrogen was injected through a rearward facing step, which was formed at the trailing face of an injection strut placed on the surface. The leading edge of the strut was sufficiently far upstream to ensure that the shock and succeeding Prandtl–Meyer expansion did not pass into the duct. Thus, the resulting duct consisted of an entry section, 114 mm long and 19×100 mm cross section, terminated by a 10-mm backward facing step, and followed by a 29×100 mm test duct 1.2 mm long (as shown in Fig. 1). The relatively small duct height had the advantage that it facilitated the detection of hydrogen combustion through the resulting pressure rise in the duct and allowed the assumption of two-dimensional flow to be used in analysis of experimental results. Numerical simulations, using the computational technique to be described, indicated that the boundary layer at the test surface was not influenced by the boundary layer on the opposing wall.

Inviscid flow calculations yielded the conditions in the entry section noted in Table 1, where they are seen to differ only slightly from those in the nozzle test flow. A further one-dimensional isentropic expansion from these conditions was used to obtain the mean flow conditions in the test duct in the absence of injection. Of course, these conditions will be modified by injection because this will change the cross-sectional area of the expanded streamtubes.

Hydrogen Injection

Hydrogen injection took place through the supersonic nozzle shown in Fig. 3. The nozzle spanned the full width of the duct, which yielded a two-dimensional flow. It was supplied from a room temperature reservoir through a solenoid operated valve, which actuated approximately 7 ms before the arrival of the test flow. The supply pressure was monitored by two piezoelectric pressure transducers, one located near each spanwise end of the step. These measured pressures, which were constant during the test time, to within ±3%. The system was precalibrated to allow the hydrogen mass flow rate to be determined from these pressures.

Tests were conducted at the four values of hydrogen mass flow shown in Table 2. The values of the ratio of hydrogen mass flow per unit slot length to the mainstream mass flow per unit area are also presented in Table 2, so that the results of this study may be

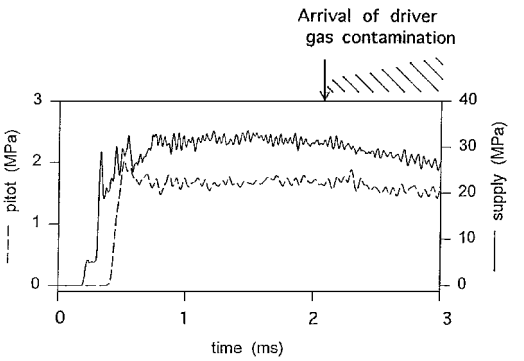

Fig. 2 Nozzle supply pressure and pitot pressure: typical test records.

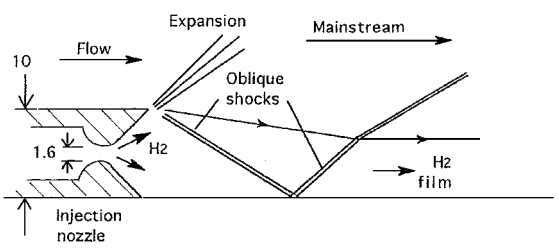

Fig. 3 Injection and formation of hydrogen film (dimensions in millimeters).

Table 2 Injected hydrogen conditions[a]

Injection condition	Mass flow, kg/s		Calculated inviscid film properties				
	Measured	Error, %	Density, kg/m^3	Velocity, m/s	Mach no.	Thickness, mm	$m_i/\rho Ul$, m $\times 10^{-4}$
1	0.015	±6	0.058	1240	1.1	2.2	3.8
2	0.029	±7	0.062	1550	1.5	3.0	7.4
3	0.043	±10	0.074	1770	1.8	3.3	11.0
4	0.057	±10	0.084	1880	2.1	4.0	14.5

[a]Estimated air boundary-layer thickness 5.8 mm.

related to a practical scheme. Although results were correlated in terms of the mass flow values, it is also useful to determine the properties of the resulting hydrogen layer that would be formed on the test surface in the absence of viscous effects. The hydrogen will undergo a supersonic expansion in the injection nozzle and a subsequent recompression to the static pressure in the mainstream within a few step heights downstream of the step. Schlieren photographs of the recompression process were presented in Ref. 2. For the three higher mass flows, the hydrogen supply pressure is high enough to produce full expansion through the nozzle to the step height. The recompression then is taken to consist of two oblique shocks, as shown in Fig. 3. By assuming such a flow, an inviscid density, velocity, Mach number, and thickness of the hydrogen film at the mean mainstream pressure were calculated and presented in Table 2, together with the mainstream air boundary-layer thickness at the same mainstream pressure, estimated by assuming that the origin of the turbulent boundary layer was 132 mm upstream of the hydrogen injection station. For the lowest mass flow, the supply pressure is insufficient to fully expand the flow in the nozzle, and the flow pattern becomes more uncertain. Thus, parameters of the inviscid hydrogen layer are provided, assuming two oblique shocks. This model generates a supersonic flow for input to the numerical calculations but, as will be seen, an alternative flow model may be required for the lowest mass flow.

Note that the calculated values in Table 2 are approximate. For instance, if the nozzle flow was not fully expanded, and instead expanded to only 60% of the step height, the values of density, velocity, and Mach number would be increased by 8, 8, and 12%, respectively, and the film thickness would be reduced by 14%.

Instrumentation

As shown in Fig. 1, the surface on which the hydrogen film was formed was instrumented to measure skin friction, heat transfer, and pressure. Heat transfer was measured by platinum thin-film gauges, mounted on a quartz substrate, and pressure was measured by PCB™ piezoelectric pressure transducers. The skin-friction gauges were manufactured in the laboratory and were of the floating element type, with the shear force transferred directly to shear on a piezoelectric element. The design and use of these gauges has been discussed in previous papers[15,16] and will be described only briefly here.

The skin-friction gauges were acceleration compensated and had a natural frequency of approximately 40 kHz. The gauges involved the use of an invar disk, 10 mm in diameter and 0.8 mm thick, as the floating element, and this was attached directly to the piezoceramic element. The polarization axis of the piezoceramic was parallel to the surface of the disk, and the maximum gauge shear response was obtained when the direction of the shear force was either parallel or opposed to the direction of polarization. Theoretically, the gauges respond only to shear, but, due to imperfections in manufacture, they were found to experience a residual response to pressure, which represented roughly 30% of the output signal in the present experiments. Also, the piezoceramic element of the gauge is sensitive to the temperature changes that can arise from heat transfer from the hot gas that enters the cavity surrounding the piezoceramic element during a test. During normal operation, the gauges were protected from this effect by heat sink material in the cavity, but because the gauges were operating in a hydrogen rich environment, the higher thermal conductivity of the hydrogen meant that there was uncertainty concerning the effectiveness of the heat sink protection and the gauges may have been subject to a heat transfer effect. It was possible to eliminate these effects by repeating the shock-tunnel tests with each gauge rotated in its mount by 180 deg, to change the polarization direction of the piezoceramic element with respect to the skin-friction force.[15] The output due to skin-friction shear was reversed by the rotation, but not the pressure and heat transfer response, and thus, by comparing outputs at 0 and 180 deg, the output due to skin-friction shear could be obtained.

Data Recording

Data were recorded and stored on a 12-bit transient digital data acquisition and storage unit with a sampling time of 1 μs. The output from the skin-friction gauges was recorded directly, whereas the output from the pressure transducers and heat transfer gauges were recorded through 4 × multiplexers, resulting in a sampling time of 4 μs for each channel. The signals from the thin-film heat transfer gauges were computer processed[17] to display the heat transfer rate. The presence of the platinum film, and the temperature rise of the quartz substrate of the gauges, caused the measured heat transfer rate to be up to 7% less than actual values,[17] but because this was barely detectable on the scale of the results presented subsequently, it was ignored in processing the data. All of the records presented were time averaged over 0.1 ms.

Experimental Data Analysis

Evidence of Combustion: Pressure and Heat Transfer

Records of pressure and heat transfer with air and with nitrogen as test gas are shown in Fig. 4. The records were obtained with pressure transducers and heat transfer gauges, which were located at the same stations as the four skin-friction gauges. Both the pressure and heat transfer rate are seen to increase when air is used with the same mass flow of hydrogen, and the increase is greatest for the downstream stations. These effects, and the relative thickness of the boundary layer and the hydrogen film seen in Table 2, are consistent with the occurrence of combustion in the boundary layer.

Distributions of pressure along the duct during the test time, with air test gas and a range of hydrogen mass flows, are presented in Fig. 5a. The step at which the hydrogen is injected would be expected to generate substantial nonuniformities in the duct flow, and these are evidenced in the pressure distributions. Nevertheless, it can be seen that the pressure rise along the duct increases as the hydrogen mass flow increases, thus providing further evidence of combustion.

Note, in Fig. 4, that the combustion induced increase in pressure and heat transfer at station B is reduced suddenly during the test time. At this station, combustion is just becoming established and is very sensitive to variations in pressure and temperature.[18] Thus, the sudden reduction may be ascribed to a combination of the local pressure gradient seen at station B in Fig. 5a and a small change in the nozzle stagnation enthalpy.

Observe, in Fig. 4, that fluctuations in heat transfer with air as test gas are somewhat greater than with nitrogen. Heat transfer records in air, without hydrogen injection, showed the same level of fluctuations as with nitrogen, which indicate that the observed fluctuations with hydrogen injected into air are due to combustion.

Local Heat Transfer and Skin-Friction Coefficients

To obtain local heat transfer and skin-friction coefficients, it is necessary to take into account variations in the mainstream conditions along the duct, as witnessed by the variations in pressure seen in Fig. 5a.

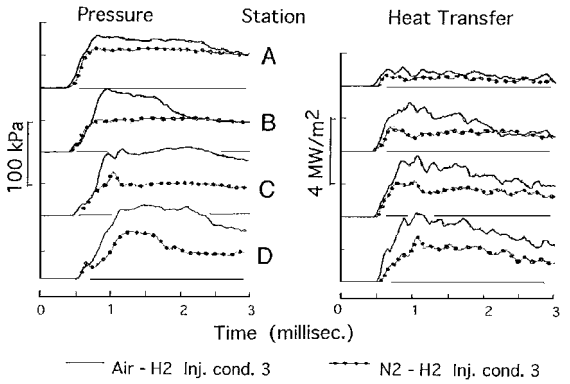

Fig. 4 Pressure and heat transfer records showing evidence of combustion.

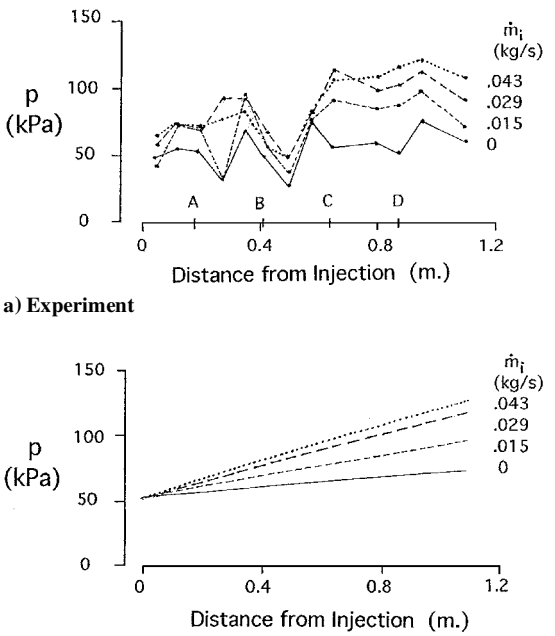

a) Experiment

b) Computational fluid dynamics

Fig. 5 Duct pressure distributions.

For heat transfer, the local Stanton number is given by

$$c_h = \dot{q}/\rho U(H_s - H_w) \tag{1}$$

and the local skin-friction coefficient is given by

$$c_f = 2\tau/\rho U^2 \tag{2}$$

Because the tests were conducted with constant values of stagnation enthalpy H_s and wall enthalpy H_w, it follows that the effect of variations in the mainstream can be taken into account through the variations in ρU and ρU^2. Boundary-layer growth and expansion and compression waves ensure variations in the local value of ρU. The variations in pressure shown in Fig. 5a are such that it is a good approximation to regard them as taking place in an isentropic flow, and it can be shown that with $\gamma = 1.35$ and a mean Mach number of 4.3, the variation of ρU and ρU^2 follows the variation of $\dot{p}^7$ and $\dot{p}^{66}$, respectively, with an error of less than 1%, for a range of pressures varying from 0.5 to 2.0 times the value at $M = 4.3$. If these pressure changes were entirely due to shock waves, an error of less than 4% would be made by regarding the flow as isentropic. Thus,

$$c_h \propto \dot{q}/\dot{p}^7 \tag{3}$$

$$c_f \propto \tau/\dot{p}^{66} \tag{4}$$

Examples of records of the variation with time of the right-hand side of Eq. (3) are presented in Fig. 6. The records were obtained

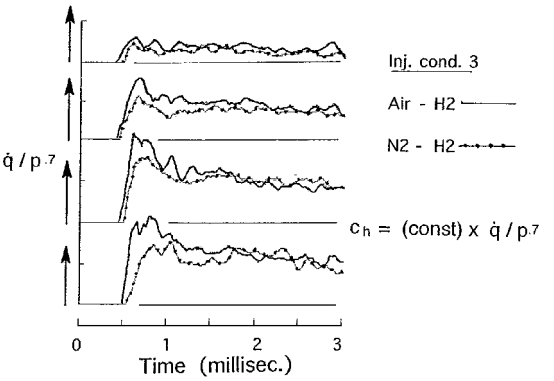

Fig. 6 Effect of combustion on Stanton number.

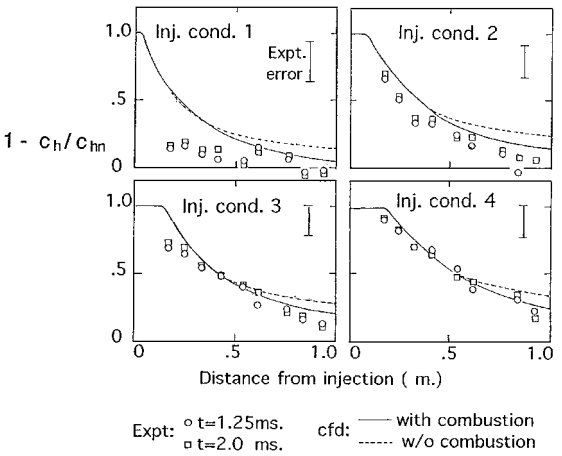

Fig. 7 Heat transfer with combustion of hydrogen film.

from the data used for Fig. 4. It can be seen that the combustion-induced increase in heat transfer evident in Fig. 4 is not reflected in a corresponding increase in the Stanton number. Similar results were obtained at all test conditions indicating that, although combustion takes place in the boundary layer, its effect on heat transfer takes place mainly through changes induced in the mainstream.

Equation (3) may be used to write the proportional reduction in Stanton number due to hydrogen injection as

$$\frac{c_{hn} - c_h}{c_{hn}} = 1 - \frac{c_h}{c_{hn}} = 1 - \frac{\dot{q}/\dot{p}^7}{(\dot{q}/\dot{p}^7)_n} \tag{5}$$

Values for $(\dot{q}/\dot{p}^7)_n$ were obtained at each station as the average of three noninjection tests. The resulting values for the proportional reduction in Stanton number for a number of injected flows of hydrogen are plotted and compared with numerical calculations in Fig. 7.

Figure 8 presents examples of the records from which the skin-friction coefficient is obtained. The output of a skin-friction gauge may be written as

$$V_0 = V_s + V_p + V_{HT}, \qquad V_{180} = -V_s + V_p + V_{HT}$$

when the gauge is aligned with the polarization direction of the piezoceramic, respectively, parallel and antiparallel to the mainstream direction. Thus, if paired shock-tunnel tests are done, with the gauge rotated 180 deg between the tests, the output due to skin friction is obtained as $V_s = (V_0 - V_{180})/2$ and using Eq. (4) as well as the relation $V_s =$ (gauge calibration constant) $\times \tau$, an output proportional to the skin-friction coefficient is obtained as

$$V_s/\dot{p}^{66} = \left(V_0/\dot{p}^{66} - V_{180}/\dot{p}^{66}\right)/2 \tag{6}$$

where it has been assumed that the pressure is unchanged between the two paired tests. In fact, the pressure did vary somewhat between tests, which gave rise to a correction to the value of $V_s/\dot{p}^{66}$, which

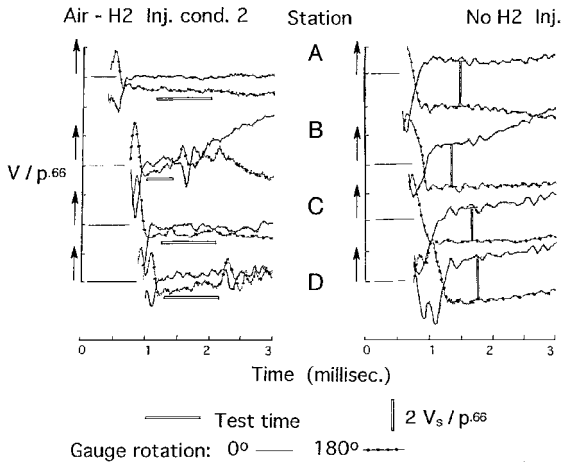

Fig. 8 Skin-friction records.

was usually less than 5% and did not exceed 9% in any of the experiments.

Figure 8 shows records obtained with hydrogen injected at condition 2 and with no hydrogen injected. No vertical scale is shown in Fig. 8, but the same scale is used for both sets of records. The records without hydrogen injection, when combined with the test duct mainstream conditions of Table 1, yield a skin-friction coefficient averaged over the four stations of $1.66 \times 10^{-3} \pm 19\%$, with a decay of 22% over the duct length. This value agrees with the measurements and theoretical correlations of Ref. 15.

Both the injection and no-injection records of Fig. 8 indicate an initial strongly negative shear, thought to be associated with boundary-layer separation during the flow starting process,[15] followed by a period of approximately steady shear. In the no-injection case, and for station A with injection, steady shear is maintained for the run duration (apart from the unexplained apparent late rise in shear at station B with 0-deg rotation and no injection). Station B with injection is indicative of the problems associated with measuring shear in a flow with combustion because the period of approximately constant shear is terminated by a large amplitude disturbance. Reference to the pressure records of Fig. 4, which are similar to those obtained for the injection condition of Fig. 8, indicates that the reduction of pressure associated with local cessation of combustion occurs at approximately the same time as these disturbances. These pressure changes may give rise to a pressure gradient across the gauge, thereby affecting the gauge output and, because this pressure gradient may be locally unsteady, the local boundary-layer profile may become distorted, with the consequences that the local shear is reduced or even reversed. Fortunately, avoiding these disturbances only affects the test time for station B because the test time for the remaining stations is terminated by the arrival of driver gas contaminant. Taking the effective origin of the test boundary layer as the point of injection, the mainstream passes 3.3 times over the distance to station B during the test time shown in Fig. 8, and this is regarded as sufficient time to ensure steady flow. More than 3.3 mainstream flow passes occur during the test time at other stations.

Comparison of the injection and no-injection records of Fig. 7 indicate that $V_s/\dot{p}^{66}$ is considerably reduced by hydrogen injection. This is converted into the proportional reduction in skin-friction coefficient through the equation

$$\frac{c_{fn} - c_f}{c_{fn}} = 1 - \frac{c_f}{c_{fn}} = 1 - \frac{V_s/\dot{p}^{66}}{(V_s/\dot{p}^{66})_n} \tag{7}$$

$V_s/\dot{p}^{66}$ is obtained as the difference between the 0- and 180-deg records, as indicated by Eq. (6) and the vertical bars in Fig. 8, and with the test times shown by the horizontal bars in Fig. 8 taken as applying at all injection conditions, the mean value of $V_s/\dot{p}^{66}$ over the test time could be ascertained. Then, by the use of Eq. (7), the proportional reduction in skin friction could be found. This skin-friction is corrected for the effect of differing pressures noted earlier and is plotted in Fig. 9.

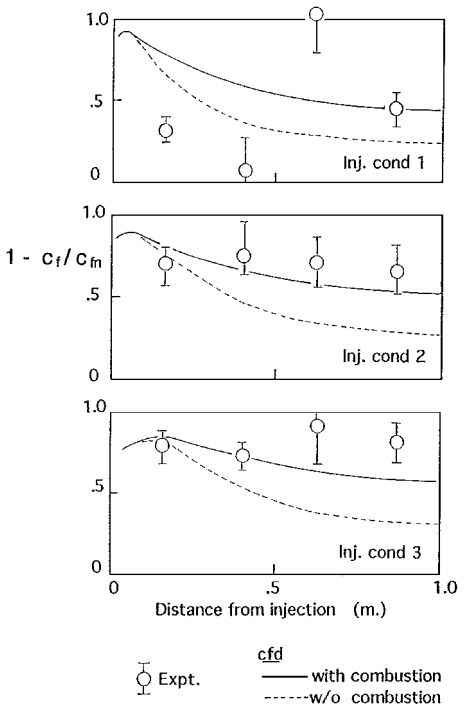

Fig. 9 Skin friction with combustion of hydrogen film.

Note that the pressure gradients that are evident in Fig. 5a produce a force on the lip face of the floating element of the gauge[15] that cannot be separated from the aerodynamic shear measurement by rotation of the gauge. Approximate estimates of the lip force effect could be obtained by assuming the pressure gradient at each station to be the mean of the measured upstream and downstream gradients and by taking the product of the resultant gradient with the lip thickness and half of the area of the floating element. When these estimates were applied to calculate the errors in the proportional reduction in skin friction, the rms errors, taken over the flow stations, were 5, 6, and 4%, respectively, for injection conditions 1, 2, and 3. These errors are incorporated in the error bars of Fig. 9.

These results can be compared with those in Ref. 15, where the skin friction was measured with hydrogen injected from a centrally located strut in a duct similar to the present one, but with a height of 48 mm. Thus, mixing and combustion occurred outside the boundary layer, producing skin-friction measurements that displayed large random fluctuations during the test time and that, when averaged over a number of tests, yielded a mean skin-friction level that was the same as that obtained in the absence of hydrogen injection. The present case, where hydrogen was injected into the boundary layer rather than the mainstream, produced very different results, with an absence of large random fluctuations and a skin-friction level reduced to well below noninjection values. Clearly the influence of boundary-layer combustion on skin friction is very different to that of mainstream combustion.

Numerical Simulation

Numerical simulations of the flow were conducted using the computer program of Ref. 11. This code is a parabolic Navier–Stokes technique, which uses a finite volume method to solve the partial differential equations and k–ε turbulence model. The fluxes of heat and shear stress to the wall were evaluated using wall functions, which assumed that the logarithmic law of the wall held in the fully turbulent region close to the wall. More detail describing the technique may be found in Ref. 11.

The simulations involved a two-dimensional flow in a duct of 30-mm constant height, with a uniform pressure across the duct, and the airstream properties given in Table 1. Hydrogen was injected as a parallel stream along one of the two bounding surfaces of the duct, with velocities, densities, and film thickness given by Table 2. The unit Reynolds number of the airstream was such that a turbulent boundary would be formed upstream of injection. This

was represented by a 5.8-mm-thick boundary layer at the entrance to the duct, with zero air velocity at the hydrogen–air interface. This boundary layer had a one-seventh power law velocity profile, and a temperature profile given by the Crocco–Busemann law (see Ref. 19). Some calculations were done with a no-friction boundary condition on the surface opposite to the one with the hydrogen film without significantly affecting the results, which indicated that the duct height was sufficient to ensure that the boundary layer on the test surface was not influenced by the boundary layer on the opposite wall. A 30-reaction, finite rate scheme, involving species O_2, N_2, H_2, H_2O, H, O, OH, HO_2, H_2O_2, N, NO, NO_2, HNO_2, and HNO, was used to model the combustion of hydrogen.[20]

The pressure distributions along the duct obtained with the numerical simulations are shown in Fig. 5b. The distributions yield approximately the same pressure increase along the duct as the experiments. Also, simulations corresponding to condition 2, with a simplified chemical reaction scheme and pressures that were allowed to vary in the transverse direction, indicated that pressure variations of the magnitude apparent in Fig. 5a did not affect the Stanton number and the skin-friction coefficient. Thus, the numerical simulations are reasonably representative of the experiments.

The computational grid used consisted of 100 points normal to the surface, and this was varied between 70 and 200 points without affecting the results of the computation. A space-marching computational scheme was used, with the step sizes in the downstream direction selected automatically as the computation progressed, resulting in approximately 40,000 steps in the downstream direction. A computation in which the number of steps was artificially increased to 82,255 yielded results that were unchanged. Therefore, it was concluded that the results were independent of the chosen computational grid size.

Discussion

Heat Transfer

The heat transfer values and the pressures obtained in the numerical simulation are combined, by following Eq. (5), to yield the reduction in local Stanton number due to hydrogen injection. Curves are plotted in Fig. 7 with hydrogen–air combustion and with reactions suppressed to show the effect of hydrogen injection without combustion. It can be seen that combustion increases the downstream heat transfer, but this increase is small, and there is only a small difference in the rise to no-injection values. The curves also show that, in accord with the observations of other investigators,[3] the rise to no-injection values occurs more gradually as the hydrogen mass flow is increased.

The experimental results for heat transfer are also presented in Fig. 7, at times of 1.25 and 2.0 ms after zero time in Figs. 4 and 6. The interval of 0.75 ms is sufficient time for the mainstream flow to pass 2.7 times over the distance from injection to the downstream heat transfer gauge and, because the Stanton number levels do not change during this period, the flow may be regarded as steady. The error bars shown were obtained by adding the rms deviation from the mean value for injection to the rms deviation for no injection and averaging the resultant over all stations, to yield the error bars shown for each injection condition.

The experimental results compare satisfactorily with the numerical simulation, except at injection condition 1. Recall the uncertainty in the calculated conditions of Table 2 for this condition; it is possible that the numerical simulation employs incorrect input variables and, thus, may not be valid at this condition. The pressure ratios at the injection nozzle suggest that the hydrogen flow may pass through a normal shock in the injection nozzle (as opposed to the two oblique shocks of Fig. 3) and emerge as a subsonic flow. The numerical analysis cannot be applied to such a situation, but the correlation of Ref. 3, where hydrogen was injected without combustion, suggests that the associated fall in the injected mass flow per unit area would ensure that, as observed, there was little reduction in the Stanton number at the heat transfer gauge stations.

Skin Friction

Curves showing the reduction in local skin friction obtained in the numerical simulations are presented in Fig. 9. The simulations yielded a value of the no-injection skin-friction coefficient, averaged over the duct length, of 2.45×10^{-3}, which compares with the measured value of 1.66×10^{-3}. Results for skin friction are often presented in terms of the mass flow of injectant divided by the no-injection skin-friction coefficient (e.g., Ref. 6), and this approach was adopted here, with the results of the simulation presented for a hydrogen mass flow 1.48 times the value used in the corresponding experiments. The levels of skin-friction coefficient were decreased by less than 10% by introducing this factor. The simulations indicate that, while the curves both with and without combustion show a reduction in skin friction as the hydrogen mass flow increases, the reduction in skin friction 1 m from injection is approximately doubled by combustion at all three injection mass flows, leading to a local skin-friction coefficient that is approximately half the no-injection value.

The measured reductions in local skin-friction coefficient are also presented in Fig. 9. As with the measured Stanton number reduction, there is a considerable difference between the measurements of skin-friction coefficient reduction and the results of numerical simulation for injection condition 1. Reference 21 indicates that, with helium injection at an injectant Mach number of 1.3, the pressure gradients evident in Fig. 5a are sufficient to modify the skin friction to the point of causing separation. Thus, the favorable pressure gradients seen in Fig. 5a at stations A and B would cause the skin friction to increase, consistent with the two upstream measurements in Fig. 9 for injection condition 1, whereas the unfavorable gradient at station C in Fig. 5a would cause a decrease in the skin friction, as seen in Fig. 9. These effects would be exacerbated if, as suggested earlier, the flow from the injection nozzle was subsonic. Observe that at the downstream skin-friction station, where Fig. 5a shows the pressure gradient to be substantially reduced in magnitude, the skin friction measurement is consistent with the numerical analysis.

The measurement of skin-friction coefficient reduction at injection conditions 2 and 3 indicate a reduction that tends to somewhat exceed the values obtained in the simulation. This may be due to an increase in the level of hydrogen–air mixing and combustion caused by the pressure disturbances evident in Fig. 5a. Apart from this effect, the measurements are in general agreement with the simulation, which indicates that there is a substantial reduction in skin friction due to combustion.

Downstream Effect

In view of the considerable reductions in skin friction seen in Fig. 9, it was of interest to determine the effect, farther downstream, of boundary-layer combustion. This effect is shown in Fig. 10, where the results are presented of applying the numerical simulation procedure to a constant pressure, flat plate flow with mainstream conditions given by the test duct conditions in Table 1. It can be seen that the trends evident in Figs. 7 and 9 are maintained, with heat transfer rising to the no-injection values a little more rapidly in the case of

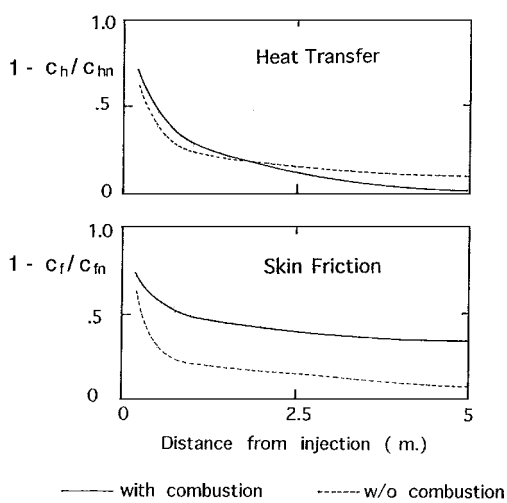

Fig. 10 Effect of boundary-layer combustion farther downstream (injection condition 2).

combustion and with the very substantial reductions in skin friction caused by boundary-layer combustion persisting over the full 5-m length.

The mass flow of hydrogen required for these reductions in skin friction is not excessive. If hydrogen was injected at condition 2 along the wall in a duct of circular cross section, with a diameter 0.3 m, at the flow conditions of Table 1, the effective equivalence ratio would be 0.37. A substantial propulsive effect can be generated by this mass flow. For example, the numerical simulation of Fig. 10 can be used to estimate the specific impulse associated with the skin-friction reduction from the no-injection level as 1057 s. Also, combustion in the boundary layer increases its displacement thickness by approximately 23 mm and, if the surface is deflected by this amount to maintain constant pressure, the pressure acting on the surface would add 400 s to the specific impulse. The specific impulse contribution arising from the injection velocity of the hydrogen is 147 s and, adding this to the other two components, yields a total of 1604 s for the hydrogen specific impulse. When combined with regenerative cooling,[22] this could make film cooling very attractive indeed as a technique for use in hypervelocity flight.

Experiments on the effect on skin friction of supersonic combustion in a plane wake in the mainstream have been reported previously.[15] They showed that, to within the accuracy of the measurements, the skin friction was not affected by combustion in the mainstream. This implies that the reductions in skin friction due to boundary-layer combustion should persist in the presence of mainstream combustion, provided that the streamwise vorticity, which is often introduced to enhance mixing in supersonic combustors, does not affect the boundary-layer flow. Further experiments to explore this possibility are planned.

Conclusion

Shock-tunnel experiments were conducted and reported to determine the effect on heat transfer and skin friction of slot injection of hydrogen when combustion of the hydrogen takes place. The height of the experimental duct was such that it was possible to use the measured pressure and heat transfer to provide evidence of combustion.

Pressure distributions indicated that substantial disturbances due to expansion and compression regions existed in the duct, and therefore, the results were analyzed in terms of the local Stanton numbers and skin-friction coefficients. The results were significantly affected by the pressure disturbances only at the lowest injection mass flow. The difficulties involved in measuring skin friction in a flow with combustion were demonstrated when rapid fluctuations in pressure caused major perturbations in the output of the skin-friction gauges. Fortunately, these fluctuations were delayed sufficiently to allow a reasonable test time for the measurements.

The results were compared with those obtained from a numerical simulation of the flow. This simulation indicated that the reduction in Stanton number due to hydrogen injection was relatively unaffected by combustion, but the reduction in skin-friction coefficient was increased, reaching approximately twice the level obtained without combustion at 1 m from injection. Except at the lowest hydrogen mass flow, the measurements of Stanton number were consistent with the simulation results, whereas the measurements of skin-friction coefficient reduction exceeded the simulation results, reaching 70–80% of the no-injection values at the maximum hydrogen mass flow.

The numerical simulation model was also used to explore the heat transfer and skin friction for a downstream distance of 5 m on a constant pressure flat plate. Hydrogen injection again yielded little difference in the Stanton number with and without combustion, but it was found that the reduction in skin friction persisted downstream with combustion, remaining at 1/3 of the no-injection value at 5 m, whereas it fell to less than 1/10 without combustion.

The effects of such factors as mainstream Mach number and enthalpy, injectant Mach number and temperature, and pressure and geometric scaling are still to be investigated. Nevertheless, the effect of boundary-layer combustion on skin friction appears to offer a means of significantly improving the flight performance of slender hypervelocity vehicles.

Acknowledgment

The authors wish to express their appreciation of the support from the Australian Research Council, who provided a grant for operation of the shock tunnel.

References

[1]Stalker, R. J., and Paull, A., "Experiments on Cruise Propulsion with a Hydrogen Scramjet," *Aeronautical Journal*, Vol. 102, No. 1011, 1998, pp. 37–43.

[2]Goldstein, R. J., Eckert, E. R. G., Tsou, F. K., and Haji-Sheikh, A., "Film Cooling with Air and Helium Injection Through a Rearward-Facing Slot into a Supersonic Airflow," *AIAA Journal*, Vol. 4, No. 6, 1966, pp. 981–985.

[3]Parthasarathy, K., and Zakkay, V., "Experimental Investigation of Turbulent Slot Injection at Mach 6," *AIAA Journal*, Vol. 8, No. 7, 1970, pp. 1302–1307.

[4]Cary, A. M., Jr., and Hefner, J. N., "Film Cooling Effectiveness in Hypersonic Turbulent Flow," *AIAA Journal*, Vol. 8, No. 11, 1970, pp. 2090, 2091.

[5]Richards, B. E., and Stollery, J. L., "Laminar Film Cooling Experiments in Hypersonic Flow," *Journal of Aircraft*, Vol. 16, No. 3, 1979, pp. 177–181.

[6]Dershin, H., Leonard, C. A., and Gallaher, W. H., "Direct Measurement of Skin Friction on a Porous Flat Plate with Mass Injection," *AIAA Journal*, Vol. 5, No. 11, 1967, pp. 1934–1939.

[7]Kenworthy, M., and Schetz, J. A., "Experimental Study of Slot Injection into a Supersonic Stream," *AIAA Journal*, Vol. 11, No. 5, 1973, pp. 585, 586.

[8]Schetz, J. A., and Van Overeem, J., "Skin-Friction Reduction by Injection Through Combinations of Slots and Porous Sections," *AIAA Journal*, Vol. 13, No. 8, 1975, pp. 971, 972.

[9]Bushnell, D. M., "Calculation of Relaxing Turbulent Boundary Layers Downstream of Tangential Slot Injection," *Journal of Spacecraft and Rockets*, Vol. 8, No. 5, 1971, pp. 550, 551.

[10]Cary, A. M., Jr., and Hefner, J. N., "Film-Cooling Effectiveness and Skin Friction in Hypersonic Turbulent Flow," *AIAA Journal*, Vol. 10, No. 9, 1972, pp. 1188–1193.

[11]Brescianini, C. P., and Morgan, R. G., "Numerical Modeling of Wall-Injected Scramjet Experiments," *Journal of Propulsion and Power*, Vol. 9, No. 2, 1993, pp. 169–175.

[12]Paull, A., Stalker, R. J., and Mee, D. J., "Experiments on Supersonic Combustion Ramjet Propulsion in a Shock Tunnel," *Journal of Fluid Mechanics*, Vol. 296, 1995, pp. 159–183.

[13]Paull, A., "A Simple Shock Tunnel Driver Gas Detector," *Shock Waves Journal*, Vol. 6, No. 5, 1996, pp. 309–312.

[14]Skinner, K. A., and Stalker, R. J., "Mass Spectrometer Measurements of Test Gas Composition in a Shock Tunnel," *AIAA Journal*, Vol. 34, No. 1, 1996, pp. 203–206.

[15]Goyne, C. P., Stalker, R. J., and Paull, A., "Shock-Tunnel Skin-Friction Measurement in a Supersonic Combustor," *Journal of Propulsion and Power*, Vol. 15, No. 5, 1999, pp. 699–705.

[16]Goyne, C. P., Paull, A., and Stalker, R. J., "Skin Friction Measurements in the T4 Shock Tunnel," *Proceedings of 21st International Symposium on Shock Waves*, edited by A. F. P. Houwing, Panther, Fyshwick, Australia, 1997, pp. 1125–1130.

[17]Schultz, D. L., and Jones, T. V., "Heat-Transfer Measurements in Short-Duration Hypersonic Facilities," AGARDograph, No. 165, 1973, pp. 6–23.

[18]Stalker, R. J., Morgan, R. G., and Paull, A., "A Shock Tunnel Investigation of Scramjet Performance with Partially Premixed Combustion," AIAA Paper 96-4534, Nov. 1996.

[19]White, F. M., *Viscous Fluid Flow*, 2nd ed. McGraw–Hill, New York, 1991, p. 541.

[20]Oldenberg, R., Chinitz, W., Friedman, M., Jaffe, R., Jachimowski, C., Rabinowitz, M., and Schott, G., "Hypersonic Combustion Kinetics," National Aerospace Plane, NASP TM-1107, Wright–Patterson AFB, OH, 1990.

[21]Juhany, K. A., and Hunt, M. L., "Flowfield Measurements in Supersonic Film Cooling Including the Effect of Shock-Wave Interaction," *AIAA Journal*, Vol. 32, No. 3, 1994, pp. 578–585.

[22]Kanda, T., Masuya, G., Ono, F., and Wakamatsu, Y., "Effect of Film Cooling/Regenerative Cooling on Scramjet Engine Performances," *Journal of Propulsion and Power*, Vol. 10, No. 5, 1994, pp. 618–624.

M. Torres
Associate Editor